Chemical Engineering Journal 242 (2014) 36–42

Contents lists available at ScienceDirect

Chemical Engineering Journal

journal homepage: www.elsevier.com/locate/cej

Synthesis and characterization of a novel MnO_x-loaded biochar and its adsorption properties for Cu^{2+} in aqueous solution

Zhengguo Song [a], Fei Lian [a,*], Zhihong Yu [a], Lingyan Zhu [b], Baoshan Xing [c], Weiwen Qiu [d]

[a] Institute of Environmental Protection, Ministry of Agriculture of China, Key Laboratory of Production Environment Quality, Ministry of Agriculture of China, Tianjin 300191, China
[b] College of Environmental Science and Engineering, Nankai University, Tianjin 300071, China
[c] Stockbridge School of Agriculture, University of Massachusetts, Amherst, MA 01003, USA
[d] The New Zealand Institute for Plant and Food Research Limited, Private Bag 4704, Christchurch 8140, New Zealand

HIGHLIGHTS

- A novel engineered sorbent (i.e., MnO_x-loaded biochar) was synthesized.
- Layered structures of MnO_x were well dispersed on the carbon surface.
- Biochar/MnO_x composite has strong sorption capacity to Cu^{2+}.
- MnO_x-loaded biochar as a low-cost sorbent may have promising environmental applications.

ARTICLE INFO

Article history:
Received 8 October 2013
Received in revised form 17 December 2013
Accepted 20 December 2013
Available online 2 January 2014

Keywords:
Biochar
MnO_x
Composite adsorbent
Cu^{2+}
Adsorption mechanism

ABSTRACT

Biochar/MnO_x composite, as a potential adsorbent, was successfully synthesized via $KMnO_4$ modification of corn straw biochar (BC) under high temperature (600 °C). Surface properties and pore structures of the MnO_x-loaded BCs were examined by complementary analytical techniques including X-ray photoelectron spectrometer, scanning electron microscopy coupled with energy dispersive X-ray spectroscopy, Fourier transform infrared spectrometer, and nitrogen adsorption measurement at 77 K. Layered structures of micro/nano-MnO_x were well dispersed on the BC surface heat-treated with 10% $KMnO_4$. Mn exhibited oxidation state between Mn^{3+} and Mn^{4+}, and the majority of surface oxygen was bonded to Mn in the forms of Mn—O (63.9%) and Mn—OH (26.3%). The MnO_x-loaded BCs exhibited much higher adsorption capacity to Cu^{2+} relative to original BC with the maximum adsorption capacity as high as 160 mg/g. The increased adsorption of Cu^{2+} on the MnO_x-loaded BCs was mainly due to the formation of inner-sphere complexes with MnO_x and O-containing groups. The stronger binding affinity of Cu^{2+} with MnO_x-loaded BCs was also supported by lower desorption rate relative to original BC. The results suggest that MnO_x-loaded BC, as a low-cost adsorbent, may have promising environmental applications.

1. Introduction

Pollution of heavy metals in water and soil has been of great concern due to their adverse effects on organisms and humans as well as nonbiodegradable nature [1]. They (e.g. Cu, Cd and Pb) are persistent in the environment and hard to remove once introduced into soil [2]. Among many remediation techniques, adsorption to high-binding adsorbents has been demonstrated to be one of the most effective and simple ways to remove heavy metals from aqueous phase or immobilize them in soil [2–4]. Due to unique surface chemistry and porous structure, activated carbons [5] and other carbon materials including carbon nanotubes [6] and graphene [7] exhibit strong adsorption affinity to heavy metals in aqueous solutions. However, their application in soil remediation and wastewater treatment in large-scale is very limited mainly because of the high cost. Thus, novel adsorbents with high adsorption capacity and abundant availability are increasingly needed for amendment of contaminated soils and/or wastewater treatment.

Biochar (BC) is produced by oxygen-limited pyrolysis of carbon-rich biomasses such as crop straw, sludge and wood [2,3,8]. Application of BC as a soil amendment is getting more attractive because of its intrinsic capacity to hold water and nutrients for plants as well as improve the physical, chemical and biological properties of soil [9,10]. Moreover, like activated carbon, BC has strong adsorption affinity to organic contaminants and heavy metals due to the porous structure and heterogeneous surface chemistry [11,12]. However, the ability of BC to adsorb contaminants depends on its physicochemical characteristics, which vary greatly

* Corresponding author.
E-mail address: lianfei2000@gmail.com (F. Lian).

1385-8947/$ - see front matter © 2013 Elsevier B.V. All rights reserved.
http://dx.doi.org/10.1016/j.cej.2013.12.061

with the raw materials and pyrolysis conditions [13]. BCs with extensive porous structure and high surface area are generally produced from the pyrolysis of source materials at high temperature (400–700 °C) [14]. The intense heat treatment inevitably results in fewer ion exchange functional groups on BC surfaces [13], which to a great extent reduces the binding sites of BC to metal ions. Thus, some efforts have been made to enhance the adsorption capacity of BC through designing BC-based composites (i.e., engineered BCs), including Fe_2O_3-coated BC [15], MgO-BC nanocomposite [16] and nano-zerovalent iron-loaded BC [17]. Zhang et al. reported that the Langmuir maximum adsorption capacity of magnetic Fe_2O_3-coated BC to As(v) is above 3000 mg/kg [15]; and MgO-BC nanocomposite exhibited high removal efficiencies to phosphate (835 mg/g) and nitrate (95 mg/g) in water [16].

Manganese oxides (MnO_x) with different phases or its composite (e.g., β-MnO_2 [18], δ-MnO_2 [19], and MnO_2-coated sand [20]) have been extensively used as adsorbents for heavy metals. MnO_2-loaded resin (D301) was demonstrated as an effective adsorbent for removal of lead and cadmium from aqueous solution [21]. Furthermore, manganese oxides were reported to have stronger binding with heavy metals (e.g., Pb) than iron oxides with similar surface area [22]. It is thus thought that the composite composed of micro/nano-MnO_x and porous BC probably has excellent performance in removal of heavy metals. Until now, however, no attempt has been made to investigate the adsorption properties of MnO_x-BC composite to heavy metals.

Therefore, the objectives of the present work are to (1) synthesize and characterize a novel engineered composite (i.e., MnO_x-loaded BC). A series of MnO_x-loaded BCs with different MnO_x coverage (2.5%, 10%, and 60%) were prepared by thermal treatment of $KMnO_4$. The prepared composites were carefully characterized for their physicochemical properties; and (2) examine adsorption capacity of MnO_x-loaded BC for Cu^{2+}, a typical heavy metal. Cu^{2+} was selected as a representative heavy metal ion since it commonly exists in the soil and aqueous environments, especially in areas of recycling wastewater for agricultural use [23].

2. Materials and methods

2.1. Synthesis of MnO_x-loaded BCs

BC was produced from corn straws through slow pyrolysis at 600 °C for 3 h in a muffle furnace under N_2 atmosphere. The obtained BC was ground to pass through a 0.15 mm sieve, and 5 g of the BC sample was soaked with 40 mL of $KMnO_4$ solution. The weight ratio of $KMnO_4$ to BC was selected as 1:40 (2.5%), 1:10 (10%) and 3:5 (60%), and thus the final products were labeled as 2.5%MBC, 10%MBC, and 60%MBC, respectively. The suspension was mixed ultrasonically for 2 h and was then oven dried at 80 °C. The mixture of BC and $KMnO_4$ was heated at 600 °C for 0.5 h under N_2 to produce MnO_x-loaded BC. The obtained samples were rinsed thoroughly with deionized water to remove impurities and dried at 80 °C. Untreated BC was also included as adsorbent for comparison.

2.2. Characterization of the samples

The bulk contents of C, H, N and S in the samples were determined using an elemental analyzer (Elementar Analysensysteme GmbH, Germany). The oxygen content was calculated based on mass balance. Ash contents were measured by heating the samples at 800 °C for 4 h. Surface chemical composition was determined using X-ray photoelectron spectrometer (XPS) (PHI 5000 VersaProbe, USA). The total amount of Mn in MnO_x-loaded BCs was determined by atomic absorption spectrophotometer (AAS, VarianAA 140/240, USA) after digested with a mixture of H_2SO_4 and oxalic acid. Surface physical morphology of the samples was examined using scanning electron microscopy (SEM) (JEOL, Japan), and localized elemental information on the chosen region was viewed with an energy dispersive X-ray spectroscopy (EDS, phoenix DX 60s) in conjunction with SEM. Their functional groups were characterized using Fourier transform infrared spectrometer (FTIR) (Nexus 870, Nicolet, USA). The BET surface area (S_{BET}), total pore volume (V_{tot}), and pore size distribution of the BCs were measured by nitrogen adsorption at 77 K using an Autosorb-1 gas analyzer (Quantachrome, USA). Point of zero surface charge (pH_{PZC}) was determined using the pH drift method [24].

2.3. Adsorption and desorption experiments

The adsorption experiments were performed in 40-mL glass vials at 25 °C. The Cu^{2+} solutions were prepared by dissolving its nitrate salt, purchased from Sigma–Aldrich, in 0.01 mol/L $NaNO_3$ as background electrolyte. The initial concentration of Cu^{2+} in the solution was in the range of 6.35–127 mg/L. 100 mg of the adsorbents and 20 mL of Cu^{2+} solutions were added to the vials. The initial pH of the solutions was adjusted to 6.0 ± 0.1 by 0.1 mol/L NaOH and HNO_3 solution. All the vials were sealed and shaken at 150 rpm in a rotary shaking incubator for 24 h to reach apparent equilibrium based on the preliminary study. Then the solutions were sampled and centrifuged, the concentrations of Cu^{2+} in the supernatant were determined using AAS. All adsorption experiments were conducted in triplicate.

For desorption experiment, 100 mg of Cu-loaded adsorbents from the adsorption test was added into 20 mL 0.01 mol/L $NaNO_3$ solution after washing and drying. The vials were shaken at 150 rpm for 24 h to reach apparent equilibrium, then the Cu^{2+} concentrations in the solution were analyzed.

2.4. Data analysis

Both Freundlich and Langmuir models were used to describe the adsorption isotherms. The two models have the following equations:

$$\text{Freundlich model}: q_e = K_F C_e^n \quad (1)$$

$$\text{Langmuir model}: q_e = Q_{\max} K_L C_e / (1 + K_L C_e) \quad (2)$$

where q_e and C_e are the equilibrium solid-phase (mg/g) and liquid-phase (mg/L) concentrations of Cu^{2+}, respectively; K_F ($mg^{1-n}\,L^n/g$) and K_L (L/mg) are the Freundlich and Langmuir adsorption affinity parameters, respectively; n is nonlinear coefficient (unitless); Q_{max} (mg/g) is the Langmuir adsorption capacity.

3. Results and discussion

3.1. Charaterization of MnO_x-loaded BCs

Relative elemental contents of C and H dramatically decreased after $KMnO_4$ modification. In contrast, bulk O content increased from 5.16% (BC) to 25.6% (60%MBC) with increasing $KMnO_4$ ratios. Measured surface O content also increased from 15.3% to 38.0% (Table 1). These data indicate that $KMnO_4$ treatment greatly increased the polarity and O-containing groups of the BC/MnO_x composite relative to original BC. The bulk content of Mn in MnO_x-loaded BCs, examined by digestion, was 6.75, 26.8, and 104 mg/g for 2.5%MBC, 10%MBC, and 60%MBC respectively, which is comparable to the calculated values (i.e., 8.48, 31.6, and 130 mg/g) based on the weight ratio of $KMnO_4$ to BC. It means that the majority of Mn (more than 80%) during the synthesizing process

Table 1
Selected physiochemical properties of the original and MnO_x-loaded BCs.

Sample	Bulk elemental composition (%)					Surface atomic composition (%)			Ash content (%)	S_{BET} (m^2/g)	Pore width (nm)	V_{tot} (cm^3/g)	pH_{PZC}
	C	H	O	N	S	C	O	Mn					
BC	85.3	1.75	5.16	0.80	2.01	75.0	15.3	–	5.02	61.0	23.7	0.036	10.0
2.5%MBC	79.7	0.43	7.95	0.77	1.99	55.3	30.2	3.05	9.18	23.8	8.92	0.013	10.3
10%MBC	73.0	0.33	10.9	0.72	1.96	39.4	40.1	7.41	13.1	3.18	70.1	0.006	10.8
60%MBC	48.6	0.24	25.6	0.48	1.58	44.2	38.0	7.80	23.4	2.28	92.2	0.005	9.7

was incorporated with original BC. Meanwhile, the increased surface Mn content (Table 1) on treated BCs demonstrates the deposition of manganese oxides. The higher ash contents are also in line with the introduction of manganese oxides into BCs.

Exposure to $KMnO_4$ under heat treatment (600 °C in N_2 for 0.5 h) heavily altered the structural properties of BC. S_{BET} of BC decreased from 61 to 2.28 m^2/g, whereas average pore width increased from 23.7 to 92.2 nm with increasing manganese oxide loading (Table 1). Manganese oxides and impurities from the decomposition of $KMnO_4$ at high temperature [25] could heavily block the micropores and reduce the surface area and pore volume of BC. On the other hand, the strong oxidative property of $KMnO_4$ may lead to the destruction of some nanopore structures and deformation from nanopores into meso-/macropores.

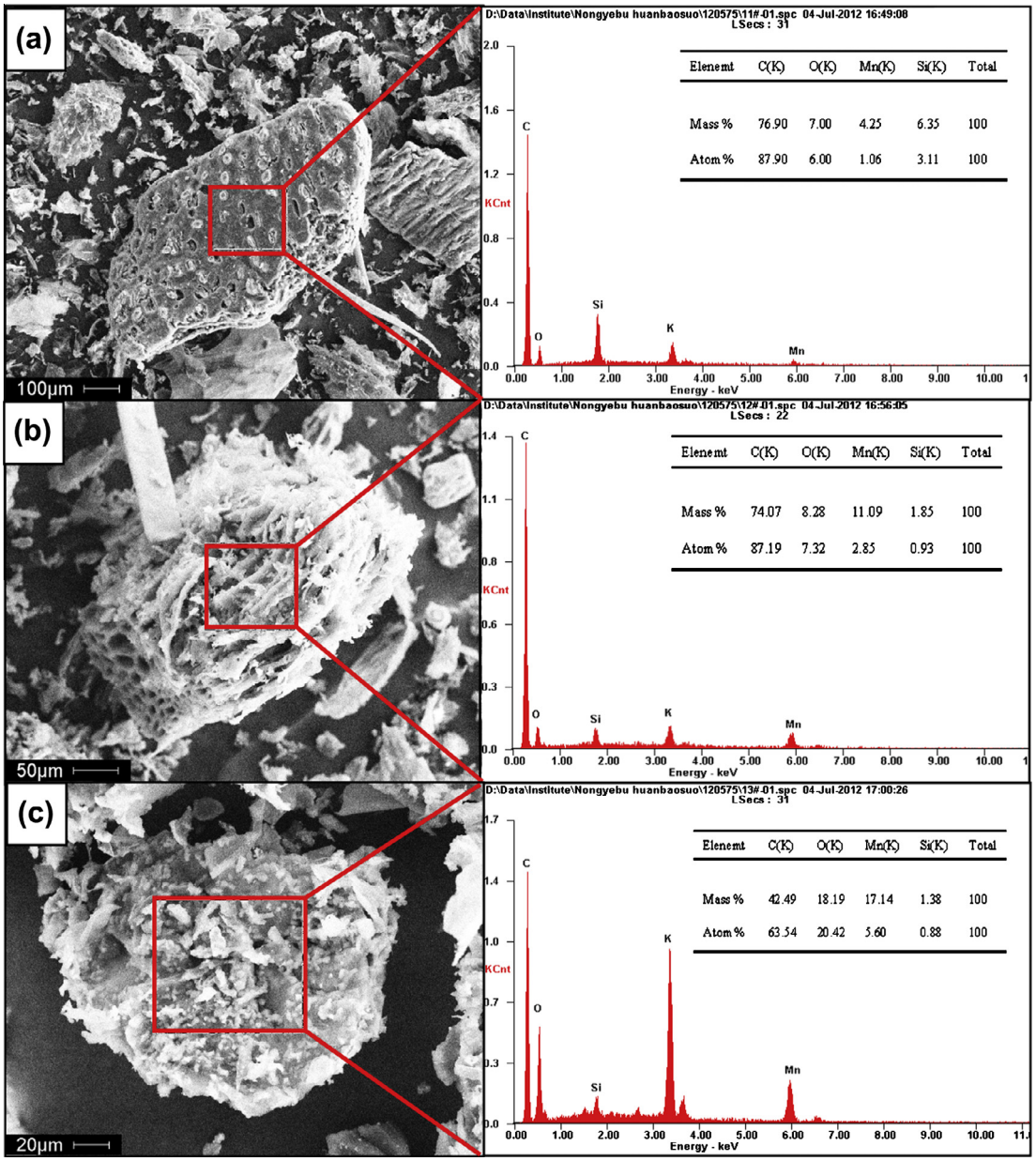

Fig. 1. SEM images of the MnO_x-loaded BCs, i.e., (a) 2.5%MBC, (b) 10%MBC and (c) 60%MBC and corresponding EDS spectra with elemental ratio of the square region inside.

Similar result was obtained with carbon nanotubes activated by KOH etching [26]. The pore-blocking effect is more remarkable for 2.5%MBC which shows much narrower average pore width (8.92 nm) relative to that of original BC (23.7 nm). With increasing $KMnO_4$ ratios, however, the oxidation effect becomes stronger and thus leads to the prominent pore widening for 10%MBC and 60%MBC.

To further examine the properties of manganese oxides on the surface of $KMnO_4$ treated BCs, SEM-EDS and XPS analysis for the samples were carried out. SEM images show that the surface of 2.5%MBC is composed of porous structures and looks much smoother compared with 10%MBC and 60%MBC (Fig. 1). It is found that layered structures of manganese oxides containing amounts of vacant sites are formed on the surface of 10%MBC, however, the carbon surface is gradually covered with agglomerates of bulk particles with manganese oxide loading increasing to 60%. The EDS analysis confirms the existence of manganese oxides on BCs, where the atomic percentages of Mn and O on the surface increase from 1.06% and 6% to 5.6% and 20.4% respectively with the enhanced $KMnO_4$ ratios (Fig. 1). The metallic state of Mn incorporated in the BC samples was examined by XPS and the spectra are compiled in Fig. 2. An obvious increase of Mn(2p) intensity was observed from the wide-scan spectra of BC after modification of $KMnO_4$ (Fig. 2a), which is consistent with the results of EDS analysis. Detailed spectra of Mn(2p) peaks are presented in Fig. 2b. The Mn(2p) binding energy values are in the range of 641.7–642.0 eV for the $KMnO_4$ treated BCs. The variation of XPS binding energies of Mn(2p) alone, between Mn^{2+} and Mn^{4+}, generally is too small (less than 1.0 eV) to precisely evaluate the Mn valence of MnO_x [27]. However, the separation between Mn($2p_{3/2}$) and Mn($2p_{1/2}$) peaks (Fig. 2a) is ~11.0 eV, indicating the Mn exhibits oxidation state between Mn^{3+} and Mn^{4+} in this study [20]. The spectra intensity of O(1s) is also greatly increased after $KMnO_4$ treatment (Fig. 2a). The O(1s) binding energy is around 530.5 eV (Fig. 2c), which is generally accepted as lattice oxygen in the form of O^{2-} (metal oxygen bond). This peak is characteristic of the oxygen in MnO_x. A similar result was obtained in the case of quartz sand modified with $KMnO_4$ [20]. Furthermore, the reconstruction of the O (1s) peak gives quantitative information on the nature of the surface oxygen groups (Fig. 2c). 10%MBC was selected as a representative, the O(1s) spectrum was divided into four peaks located at 530.1, 531.4, 532.4 and 533.2 eV, respectively [28]. The peaks could be assigned to manganese oxide (Mn—O), hydroxyl bonding to Mn (Mn—OH), hydroxyl on BC surface (C—OH) as well as chemisorbed water [28]. The majority of surface oxygen is bonded to Mn in the forms of Mn—O (63.9%) and Mn—OH (26.3%), which would provide abundant active adsorption sites for Cu^{2+}.

3.2. Adsorption properties of Cu^{2+} on the adsorbents

Adsorption isotherms of Cu^{2+} on the original and MnO_x-loaded BCs are shown in Fig. 3. The adsorption data were fitted to Freundlich and Langmuir models respectively and the fitting parameters are listed in Table 2. Langmuir model provides better fit than Freundlich model (R^2 = 0.93–0.99 versus R^2 = 0.86–0.97, Table 2), which indicates that surface coverage plays a dominating role in the adsorption of Cu^{2+} in this work. Langmuir model has been commonly used to fit the adsorption of heavy metal ions on geosorbents, black carbons and carbon nanotubes in previous studies [29]. Thus, the adsorption data are discussed here mainly based on the Langmuir model fitting results.

Among the adsorbents, 10%MBC exhibits the highest adsorption capacity (Q_{max}, 160.3 mg/g) for Cu^{2+}, which is more than 8 times of the original BC (19.6 mg/g, Table 2). The reported adsorption capacities of Cu^{2+} by BCs derived from various raw materials

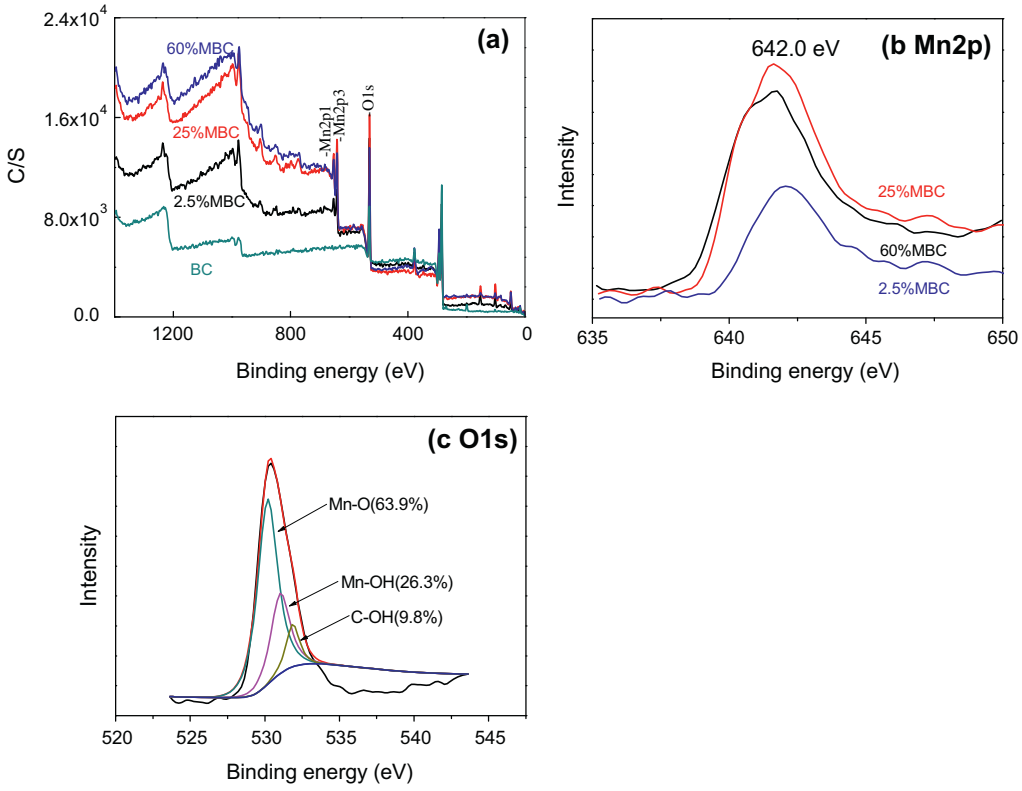

Fig. 2. (a) XPS wide scan of the original and MnO_x-loaded BCs, (b) XPS showing Mn2p core level in MnO_x-loaded BCs and (c) XPS showing O1s core level in 10%MBC along with its deconvolution.

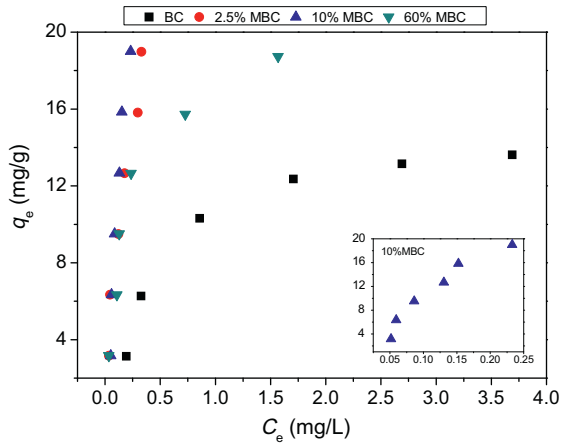

Fig. 3. Adsorption isotherms of Cu^{2+} on the original and MnO_x-loaded BCs.

including crop straws and livestock manure are in the range of several mg/g to ~90 mg/g [8,29,30]. Another study showed that hydrothermally produced chars derived from pinewood and rice husk had adsorption capacity of 25.2 and 22.6 mg/g for Cu^{2+}, respectively [31]. Besides, Wilson et al. [32] reported that the adsorption capacity of two commercial activated carbons for Cu^{2+} was ~56 and 65 mg/g at pH 4.8, more than 2 times lower than that of 10%MBC. Apparently, our data indicate that coating with MnO_x could greatly enhance the adsorption of Cu^{2+} on BCs. Similarly, a recent study developed graphene nanosheet/MnO_2 composites to remove Cu^{2+} and Pb^{2+} from aqueous solution [28]. The adsorption capacity of the composites for Cu^{2+} was reported to be ~103 mg/g, which amounts to 64% of that of 10%MBC in current work. The higher adsorption capacity of MnO_x-loaded BC may be understood by the fact that porous BC exhibits higher BET surface area than graphene sheet, and could provide more surface sites for micro/nano-MnO_x loading, which leads to stronger sorption for Cu^{2+} ions. In terms of practical use consideration, BC is much cheaper and more easily obtained in large quantities relative to graphene sheet and activated carbon. Thus, BC may be an excellent candidate for effective and low-cost support for nanomaterial-carbon composites in environmental applications.

Note that, compared to 2.5%MBC and 10%MBC, 60%MBC has lower adsorption capacity (Q_{max}, 18.5 mg/g) to Cu^{2+}, indicating that appropriate surface loading of MnO_x on BC is one of the critical factors in controlling the adsorption capacity of Cu^{2+} on MnO_x-loaded BC. Previous studies demonstrated that high-energy adsorption sites for metal ions are mainly located on the edges, defects and vacant sites in the interlayer of manganese oxides [33]. However, excessive loaded MnO_x (e.g., 60%MBC) are likely to form agglomerates of bulk particles on the carbon surface as reflected by the SEM images (Fig. 3c). Thus, many adsorption sites on the edges and interlayers of nano/micro-sized MnO_x structures could be easily covered by the bulky MnO_x particles. Accordingly, 10%MBC has much more Cu^{2+} binding sites on the surface than 60%MBC, thus higher adsorption capacity to Cu^{2+}. However, it is noted that the binding affinity is stronger for 60%MBC relative to the original BC (justified by the values of K_L and K_F, Table 2), especially at low aqueous concentrations of Cu^{2+} (Fig. 3). It is indicated that the adsorption efficiency of 60%MBC to Cu^{2+} was higher relative to original BC in spite of its comparable Cu^{2+} adsorption capacity on the unit mass basis.

To better understand the differences in binding energy for Cu^{2+} between original and MnO_x-loaded BCs, desorption of Cu^{2+} was conducted in $NaNO_3$ solution. Fig. 4 clearly reveals that desorption of Cu^{2+} from all the samples decreases greatly with increasing surface MnO_x content. The maximum desorption rate of Cu^{2+} (% = desorbed amount of Cu^{2+}/corresponding adsorbed amount of Cu^{2+}) was calculated and followed the order of BC (11.6%) > 2.5%MBC (7.9%) > 10%MBC (0.7%) > 60%MBC (0.66%). The results indicate that coating with micro/nano-MnO_x could greatly improve the binding affinity of Cu^{2+} on BC surface and thus decrease its desorption from BC. The adsorbed metal ions which can be desorbed by un-buffered salt solution (e.g., $NaNO_3$ in this study) are generally considered as non-specifically (exchangeable) adsorbed ions [34]. Thus the desorption data suggest that coating with MnO_x increases the relative contribution of specific adsorption of Cu^{2+} with BCs. It is reasonable to assume that MnO_x-BCs would be more effective compared with original BCs in retarding the transport of heavy metals in aquatic environment and in engineered processes (e.g., water and wastewater treatment).

3.3. Adsorption mechanisms of Cu^{2+} on the MnO_x-loaded BCs

In order to elucidate the adsorption mechanisms, FTIR measurements were performed to compare the different adsorption of Cu^{2+} on original BC and MnO_x-loaded sample (i.e., 10%MBC) (Fig. 5). The broad band around 3442 cm^{-1} and more prominent peak at 1385 cm^{-1} are associated with υ(–OH) vibration in hydroxyl groups [27,35]. The peaks at 2927 and 2856 cm^{-1} correspond to the CH_2 deformation vibration [36], and the signal at 1103 cm^{-1} can be assigned to the C—O groups [37]. The regions from 1526 to 1825 cm^{-1} are ascribed to aromatic groups (e.g., C=C) and carbonyl/carboxyl C=O stretching vibration. Noticeably, modification with $KMnO_4$ greatly increased the contents of O-containing groups of BC, reflected by the enhanced band intensities such as 3442 and 1103 cm^{-1}, especially for the O—H bending at 1385 cm^{-1} (Fig. 5). After reaction with Cu^{2+}, the peak at 1385 cm^{-1} weakened greatly for 10%MBC, however, a slight increase was observed with the original BC sample. This indicates that the adsorption affinity of Cu^{2+} on the two adsorbents is different from each other. It can be explained by the fact that the higher absorption peak at 1385 cm^{-1} is attributed to OH deformation vibrations of hydrated MnO_x on the surface of 10%MBC [27]. The hydroxyl groups were highly consumed in the adsorption of Cu^{2+} to form strong uni/multi-dentate inner-sphere complexes (e.g., Mn—O—Cu), leading to the decrease of O—H signal at 1385 cm^{-1}. However, the band at 1385 cm^{-1} for original BC is probably due to O—H bending of phenol or C—O stretching of COOH [35]. In contrast, the stronger binding affinity between Cu^{2+} and MnO_x leads to more significant variation of the peak at 1385 cm^{-1}. The spectra results provide more evidence on

Table 2
Regression parameters of Cu^{2+} adsorption isotherms based on Freundlich and Langmuir models.

Adsorbent	Freundlich			Langmuir		
	K_F (mg^{1-n} L^n/g)	n	R^2	Q_{max} (mg/g)	K_L (L/mg)	R^2
BC	7.03(0.54)	0.53(0.07)	0.953	19.6(1.27)	0.60(0.09)	0.991
2.5%MBC	13.6(1.14)	0.40(0.09)	0.863	54.7(30.6)	1.14(0.84)	0.966
10%MBC	68.0(18.0)	0.97(0.15)	0.935	160.3(28.3)	1.08(0.48)	0.940
60%MBC	36.9(4.94)	0.81(0.09)	0.971	18.5(2.08)	3.42(1.07)	0.925

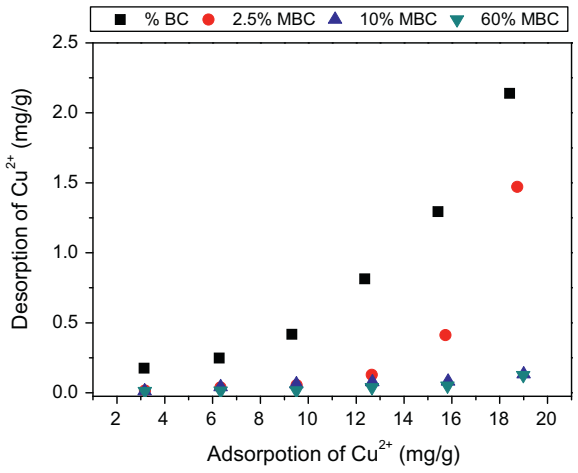

Fig. 4. Desorption fractions of pre-adsorbed Cu^{2+} on the original and MnO_x-loaded BCs.

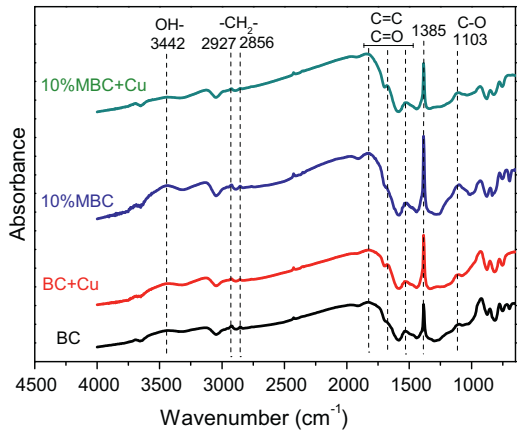

Fig. 5. FTIR spectra of the original BC and 10%MBC as well as after adsorption of Cu^{2+}.

the strong interactions between Cu^{2+} and MnO_x on the surface of treated BCs. Similar to our observation, hydroxyl groups on graphene nanosheet/MnO_2 composites were also heavily changed after Cu^{2+} adsorption [28], where formation of monodentate complexes on surface of the composites was proposed to play a dominant role in the adsorption based on the results of XPS and XRD [28]. It was also reported that adsorption of Cu^{2+} on crop residue BCs was mainly through carboxylic and hydroxylic groups, and adsorption capacities were roughly positively correlated with their oxygen contents [23,29].

Although complexation is strong between Cu^{2+} and MnO_x as well as O-containing groups on BCs, adsorption due to cation-π interaction should be also considered. It is reported that graphenic carbon atoms exhibit a basic character which allows them to serve as adsorption sites for positively charged hydrated metal cations in aqueous solutions [6]. With increasing pyrolysis temperature, the structure of BC is gradually converted from a predominantly amorphous characteristic into a turbostratic char material mainly composed of disordered graphitic crystallites [38]. An abundance of polarized π-electron is known to be associated with the graphene sheets of plant-derived BCs [39]. Previous study suggested that Cd^{2+} adsorption on plant-derived BCs produced above 350 °C occurred predominantly via cation-π bonding with electron-rich domains on aromatic structures [39]. Similarly, Cu^{2+} was also observed to be adsorbed on carbon nanotubes through strong cation-π interaction at solution pH 6.5 [40]. The BCs used in this work was produced at 600 °C from corn straw, which may contain abundant graphene-like domains on the carbon surface [38]. Thus, cation-π interaction could be another important contributor to Cu^{2+} adsorption on the original BC. Meanwhile, it is speculated that the rest of BC surface unstained by manganese oxides, especially for 2.5%MBC and 10%MBC, could also interact with Cu^{2+} through cation-π bonding. However, for 60%MBC, the much higher coverage by manganese oxides and impurities from pyrolysis of $KMnO_4$ to a greater extent altered the surface structure of BC and influenced the formation of delocalized-π bond in graphene-like domains and thus the cation-π interaction with Cu^{2+} ions. Therefore, it is reasonable to speculate that the weakened cation-π interaction could also be used to partly explain the lower adsorption capacity (Q_{max}) of Cu^{2+} on 60%MBC compared to 2.5%MBC and 10%MBC.

Our pH drift experiment suggests that both original and MnO_x-loaded BCs are positively charged in the tested pH (~6.0) due to their high pH_{PZC} values (around 10, Table 1), which is consistent with the literature that BC generally has an alkaline pH [9]. Meanwhile, our previous study [41] suggested that Cu^{2+} is the main species at suspension pH below 6. Thus, cation exchange with protonated functional groups (e.g., —OH and —COOH) of BCs could partly contribute to Cu^{2+} adsorption in this work, which is evidenced by the slight decrease of equilibrium aqueous pH (i.e., pH decreases from 6.0 to ~5.7) with increasing Cu^{2+} adsorption.

4. Conclusions

A novel engineered adsorbent (i.e., MnO_x-loaded BC) was successfully synthesized via $KMnO_4$ modification of corn straw BC in a nitrogen atmosphere at 600 °C. Layered structures of micro/nano-MnO_x were well dispersed on the BC surface heat-treated with 10% $KMnO_4$. The unique nanostructure makes the MnO_x-loaded BCs has much stronger adsorption capacity for Cu^{2+} than original BC with the maximum adsorption capacity as high as 160 mg/g. The increased adsorption of Cu^{2+} on the MnO_x-loaded BCs was mainly due to the formation of surface complexes with MnO_x and O-containing groups. Besides, other mechanisms including cation-exchange and cation-π bonding may also be involved in the Cu^{2+} adsorption. Meanwhile, the desorption data evidenced that the adsorbed Cu^{2+} on MnO_x-loaded BCs was more stable than on original BC, indicating that MnO_x/BC composites, as a low-cost adsorbent, may be more effective in various environmental applications, such as wastewater treatment or immobilization of heavy metals (e.g., Cu^{2+}) in contaminated soils.

Acknowledgements

This research was supported by The National Science Foundation of China (41273136, 41203083) and Central Public Research Institutes Basic Funds for Research and Development (Agro-Environmental Protection Institute, Ministry of Agriculture (2012-SZJJ-lds).

References

[1] K.E. Giller, E. Witter, S.P. McGrath, Toxicity of heavy metals to microorganisms and microbial processes in agricultural soils: a review, Soil Biol. Biochem. 30 (1998) 1389–1414.
[2] J. Jiang, R. Xu, T. Jiang, Z. Li, Immobilization of Cu(II), Pb(II) and Cd(II) by the addition of rice straw derived biochar to a simulated polluted Ultisol, J. Hazard. Mater. 229 (2012) 145–150.
[3] H. Lu, W. Zhang, Y. Yang, X. Huang, S. Wang, R. Qiu, Relative distribution of Pb(2+) sorption mechanisms by sludge-derived biochar, Water Res. 46 (2012) 854–862.
[4] L. Beesley, M. Marmiroli, The immobilisation and retention of soluble arsenic, cadmium and zinc by biochar, Environ. Pollut. 159 (2011) 474–480.

[5] Y.F. Jia, K.M. Thomas, Adsorption of cadmium ions on oxygen surface sites in activated carbon, Langmuir 16 (2000) 1114–1122.
[6] H.-H. Cho, K. Wepasnick, B.A. Smith, F.K. Bangash, D.H. Fairbrother, W.P. Ball, Sorption of aqueous Zn II and Cd II by multiwall carbon nanotubes: the relative roles of oxygen-containing functional groups and graphenic carbon, Langmuir 26 (2010) 967–981.
[7] T.S. Sreeprasad, S.M. Maliyekkal, K.P. Lisha, T. Pradeep, Reduced graphene oxide–metal/metal oxide composites: facile synthesis and application in water purification, J. Hazard. Mater. 186 (2011) 921–931.
[8] X. Chen, G. Chen, L. Chen, Y. Chen, J. Lehmann, M.B. McBride, A.G. Hay, Adsorption of copper and zinc by biochars produced from pyrolysis of hardwood and corn straw in aqueous solution, Bioresource Technol. 102 (2011) 8877–8884.
[9] B. Glaser, J. Lehmann, W. Zech, Ameliorating physical and chemical properties of highly weathered soils in the tropics with charcoal – a review, Biol. Fert. Soils 35 (2002) 219–230.
[10] J. Lehmann, J. Gaunt, M. Rondon, Biochar sequestration in terrestrial ecosystems – a review, Mitig. Adapt. Strat. Global 11 (2006) 395–419.
[11] S.M. Martin, R.S. Kookana, L. Van Zwieten, E. Krull, Marked changes in herbicide sorption–desorption upon ageing of biochars in soil, J. Hazard. Mater. 231 (2012) 70–78.
[12] M. Uchimiya, S. Chang, K.T. Klasson, Screening biochars for heavy metal retention in soil: role of oxygen functional groups, J. Hazard. Mater. 190 (2011) 432–441.
[13] K. Sun, K. Ro, M.X. Guo, J. Novak, H. Mashayekhi, B.S. Xing, Sorption of bisphenol A, 17 alpha-ethinyl estradiol and phenanthrene on thermally and hydrothermally produced biochars, Bioresource Technol. 102 (2011) 5757–5763.
[14] B. Liang, J. Lehmann, D. Solomon, S. Sohi, J.E. Thies, J.O. Skjemstad, F.J. Luizao, M.H. Engelhard, E.G. Neves, S. Wirick, Stability of biomass-derived black carbon in soils, Geochim. Cosmochim. Acta 72 (2008) 6069–6078.
[15] M. Zhang, B. Gao, S. Varnoosfaderani, A. Hebard, Y. Yao, M. Inyang, Preparation and characterization of a novel magnetic biochar for arsenic removal, Bioresource Technol. 130 (2013) 457–462.
[16] M. Zhang, B. Gao, Y. Yao, Y. Xue, M. Inyang, Synthesis of porous MgO-biochar nanocomposites for removal of phosphate and nitrate from aqueous solutions, Chem. Eng. J. 210 (2012) 26–32.
[17] Z. Liu, F.-S. Zhang, Nano-zerovalent iron contained porous carbons developed from waste biomass for the adsorption and dechlorination of PCBs, Bioresource Technol. 101 (2010) 2562–2564.
[18] D. Zhao, X. Yang, H. Zhang, C. Chen, X. Wang, Effect of environmental conditions on Pb(II) adsorption on β-MnO2, Chem. Eng. J. 164 (2010) 49–55.
[19] S.S. Tripathy, S.B. Kanungo, Adsorption of Co^{2+}, Ni^{2+}, Cu^{2+} and Zn^{2+} from 0.5 M NaCl and major ion sea water on a mixture of δ-MnO_2 and amorphous FeOOH, J. Colloid Interface Sci. 284 (2005) 30–38.
[20] R. Han, W. Zou, Z. Zhang, J. Shi, J. Yang, Removal of copper(II) and lead(II) from aqueous solution by manganese oxide coated sand – I. Characterization and kinetic study, J. Hazard. Mater. 137 (2006) 384–395.
[21] L. Dong, Z. Zhu, H. Ma, Y. Qiu, J. Zhao, Simultaneous adsorption of lead and cadmium on MnO_2-loaded resin, J. Environ. Sci. 22 (2010) 225–229.
[22] S.E. O'Reilly, M.F. Hochella, Lead sorption efficiencies of natural and synthetic Mn and Fe-oxides, Geochim. Cosmochim. Ac 67 (2003) 4471–4487.
[23] G.-C. Chen, X.-Q. Shan, Y.-S. Wang, B. Wen, Z.-G. Pei, Y.-N. Xie, T. Liu, J.J. Pignatello, Adsorption of 2,4,6-trichlorophenol by multi-walled carbon nanotubes as affected by Cu(II), Water Res. 43 (2009) 2409–2418.
[24] H. Valdés, M. Sánchez-Polo, J. Rivera-Utrilla, C. Zaror, Effect of ozone treatment on surface properties of activated carbon, Langmuir 18 (2002) 2111–2116.
[25] F.H. Herbstein, M. Kapon, A. Weissman, Old and new studies of the thermal decomposition of potassium permanganate, J. Therm. Anal. 41 (1994) 303–322.
[26] L. Ji, Y. Shao, Z. Xu, S. Zheng, D. Zhu, Adsorption of monoaromatic compounds and pharmaceutical antibiotics on carbon nanotubes activated by KOH etching, Environ. Sci. Technol. 44 (2010) 6429–6436.
[27] S. Xing, C. Hu, J. Qu, H. He, M. Yang, Characterization and reactivity of MnO_x supported on mesoporous zirconia for herbicide 2,4-D mineralization with ozone, Environ. Sci. Technol. 42 (2008) 3363–3368.
[28] Y. Ren, N. Yan, J. Feng, J. Ma, Q. Wen, N. Li, Q. Dong, Adsorption mechanism of copper and lead ions onto graphene nanosheet/delta-MnO_2, Mater. Chem. Phys. 136 (2012) 538–544.
[29] X. Tong, J. Li, J. Yuan, R. Xu, Adsorption of Cu (II) by biochars generated from three crop straws, Chem. Eng. J. 172 (2011) 828–834.
[30] X. Xu, X. Cao, L. Zhao, H. Wang, H. Yu, B. Gao, Removal of Cu, Zn, and Cd from aqueous solutions by the dairy manure-derived biochar, Environ. Sci. Pollut. R 20 (2013) 358–368.
[31] Z. Liu, F.-S. Zhang, Removal of copper (II) and phenol from aqueous solution using porous carbons derived from hydrothermal chars, Desalination 267 (2011) 101–106.
[32] K. Wilson, H. Yang, C.W. Seo, W.E. Marshall, Select metal adsorption by activated carbon made from peanut shells, Bioresource Technol. 97 (2006) 2266–2270.
[33] M. Zhu, M. Ginder-Vogel, D.L. Sparks, Ni(II) Sorption on biogenic Mn-oxides with varying Mn octahedral layer structure, Environ. Sci. Technol. 44 (2010) 4472–4478.
[34] R.K. Xu, S.C. Xiao, A.Z. Zhao, G.L. Ji, Effect of Cr(VI) anions on adsorption and desorption behavior of Cu(II) in the colloidal systems of two authentic variable charge soils, J. Colloid Interface Sci. 284 (2005) 22–29.
[35] F. Lian, B.S. Xing, L.Y. Zhu, Comparative study on composition, structure, and adsorption behavior of activated carbons derived from different synthetic waste polymers, J. Colloid Interface Sci. 360 (2011) 725–730.
[36] B.L. Chen, Z.M. Chen, S.F. Lv, A novel magnetic biochar efficiently sorbs organic pollutants and phosphate, Bioresource Technol. 102 (2011) 716–723.
[37] X.L. Wang, B.S. Xing, Sorption of organic contaminants by biopolymer-derived chars, Environ. Sci. Technol. 41 (2007) 8342–8348.
[38] M. Keiluweit, P.S. Nico, M.G. Johnson, M. Kleber, Dynamic molecular structure of plant biomass-derived black carbon (biochar), Environ. Sci. Technol. 44 (2010) 1247–1253.
[39] O.R. Harvey, B.E. Herbert, R.D. Rhue, L.J. Kuo, Metal interactions at the biochar-water interface: energetics and structure-sorption relationships elucidated by flow adsorption microcalorimetry, Environ. Sci. Technol. 45 (2011) 5550–5556.
[40] D. Wu, B. Pan, M. Wu, H. Peng, D. Zhang, B. Xing, Coadsorption of Cu and sulfamethoxazole on hydroxylized and graphitized carbon nanotubes, Sci. Total. Environ. 427 (2012) 247–252.
[41] F. Lian, Z. Song, Z. Liu, L. Zhu, B. Xing, Mechanistic understanding of tetracycline sorption on waste tire powder and its chars as affected by Cu^{2+} and pH, Environ. Pollut. 178 (2013) 264–270.